Université de Mons
Faculté Polytechnique – Service de Mécanique Rationnelle, Dynamique et Vibrations
31, Bld Dolez - B-7000 MONS (Belgique)
065/37 42 15 – georges.kouroussis@umons.ac.be

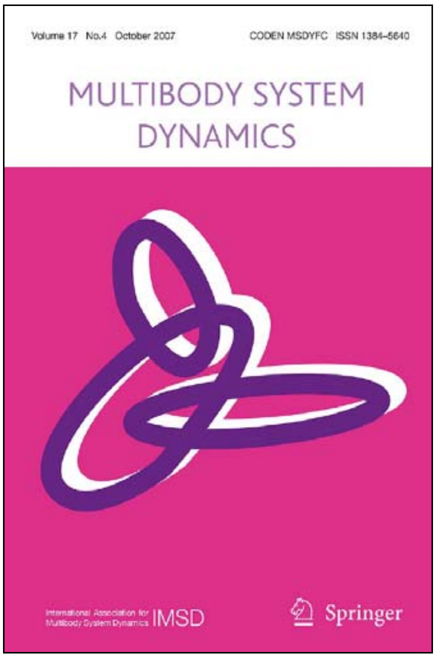

B. Olivier, O. Verlinden, G. Kouroussis, Comparison of X–T and X–X co-simulation techniques applied on railway dynamics, *Multibody System Dynamics*, 55(1-2): 39–56, 2022.

Multibody System Dynamics (2022) 55:39–56
https://doi.org/10.1007/s11044-022-09821-4

Comparison of X–T and X–X co-simulation techniques applied on railway dynamics

Bryan Olivier[1] · Olivier Verlinden[1] · Georges Kouroussis[1]

Received: 14 September 2021 / Accepted: 17 March 2022 / Published online: 5 April 2022

Abstract
Co-simulation techniques start to be of high interest when building a vehicle–track–soil model dedicated to ground-borne vibrations' assessment. If this model includes a relatively comprehensive representation of the vehicle, track, and soil subdomains, different solvers may be used to simulate them. In this paper, the vehicle and track are modeled in a multibody dedicated software and the soil is simulated in a finite element analysis software. The aim of this paper is to investigate the effect of displacement/force and displacement/displacement co-simulation types in the case of coupled railway-soil dynamics. Both Jacobi and Gauß–Seidel approaches are used without iterations and using a zeroth-order hold extrapolation of the coupling variables. The modeling of the subdomains is described and an implementation of the co-simulation is proposed. By observing the ground and vehicle motions, as well as the peak particle velocity of the soil with respect to the distance from the track, it is stated that the choice of displacement/force or displacement/displacement co-simulation type has a significant effect on the results. Indeed, while the displacement/displacement type offers a larger stability region than the displacement/force type, the accuracy of the results is more heavily affected.

Keywords Solver-coupling · Co-simulation · Railway dynamics · Finite element analysis · Ground-borne vibrations

1 Introduction

The displacement of heavy vehicles is usually an important factor in the generation of ground-borne vibrations. In the case of railway dynamics, the vibrations propagating through the soil may disturb the surrounding environment, leading to disturbance or discomfort and even to structural damages in the buildings surrounding the track [1]. The estimation

✉ B. Olivier
bryan.olivier@umons.ac.be

O. Verlinden
olivier.verlinden@umons.ac.be

G. Kouroussis
georges.kouroussis@umons.ac.be

1 Department of Theoretical Mechanics, Dynamics and Vibrations, Faculty of Engineering, University of Mons, Place du Parc 20, 7000 Mons, Belgium

of the ground-borne vibrations is therefore of high interest either when building a new track or when constructing a building nearby a railway track. In order to efficiently assess the vibration level generated by a moving train, a numerical model can be built, including a sufficiently comprehensive model of the soil. Since the soil and vehicle are two fundamentally different subsystems, a co-simulation technique coupling two software packages especially dedicated to each subsystem (one for the vehicle and one for the soil dynamics) is investigated in this paper.

The interaction of railway vehicles with the surrounding structure is a frequently considered and discussed subject in the literature. Not necessarily concerning ground-borne vibration assessment, plenty of different vehicle-structure models were successively built over the decades. Regarding methods applied in time-domain only, there exist one-step methods [2, 3] in which the whole system is usually simulated in a same solver. Due to the considerable behavioral differences between the soil, track, and vehicle, decoupling–recoupling techniques were already tested. Zhai et al. [4, 5], Yang et al. [6], and Kouroussis et al. [7–9] developed two-step approaches (one for the forces' estimation and one for the forces' application) that differ by the way they include the track modeling in both steps.

During the last decades, co-simulation techniques were largely studied on different kinds of multiphysics systems from the simplest possible, the double oscillator [10–14], to multibody-hydraulic systems [15, 16], multibody-electric systems [17], or even multibody and finite element analysis coupling [18–21]. Due to its intrinsic applicability to multiphysics systems, co-simulation remains highly used in a wide range of fields. Gomes made a general review of the usage of co-simulation applied to multiphysics systems [22, 23].

Co-simulation was already used in the specific case of railway dynamics while focusing on the interaction between the vehicle and the track [18, 21, 24–26]. Most of them usually focus on the vehicle and track dynamics without necessarily taking into account an accurate model of the soil (for vibration assessment). The model studied in this work, whose subsystems composition is detailed in [27], includes a three-dimensional finite element modeling of the soil ($\approx$ 500.000 degrees of freedom, in a finite element analysis software) co-simulating with a two-dimensional vehicle/track model ($\approx$ 500 degrees of freedom in a multibody dedicated in-house software). In the present paper, both MBS and FEM software packages were kept from [27] in order to produce a valid comparison. Originally, these software tools were used to build a two-step (without co-simulation) model [7–9].

In reality, the whole problem is obviously completely coupled. However, in order to use the dedicated software for the soil and vehicle subsystems, a choice has to be made regarding the split location and therefore the location of the track (rail–railpads–sleepers–ballast) in these subsystems. Unlike the approaches in [21, 24] that split the system at the wheel/rail contact level, the choice was made to split the system at the ballast level, so that the track is completely included in the vehicle subsystem. Consequently, opting for applied-force co-simulation techniques and using the ballast as the coupling element between the subsystems leads to two main categories of coupling type defining the nature of the coupling variable that each subsystem will receive from the other one every macrotimestep. Generally speaking, a subsystem may receive a kinematic quantity (displacement and velocity) and send either a kinematic quantity as well or a force quantity. For the sake of simplicity and as already stated by Wang for gluing techniques [28], the kinematic and force quantities will be denoted, in the rest of the paper, by X and T, respectively. Besides providing information about the modeling of the co-simulated vehicle–track–soil system, the aim of this paper is to investigate the effect of X–X and X–T co-simulation coupling types in the specific case of railway dynamics. Both considered configurations are depicted in Fig. 1.

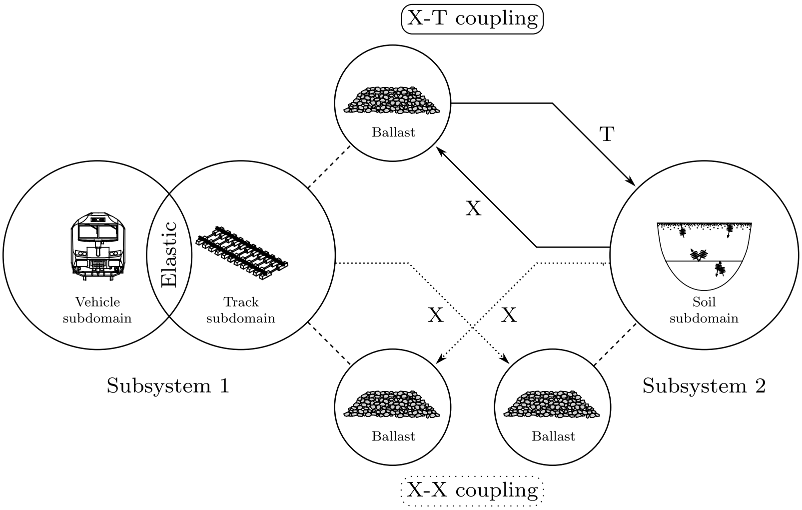

Fig. 1 Illustration of both X–T (——) and X–X (······) co-simulation coupling types for the considered vehicle–track–soil model. The dashed (- - -) lines represent an inclusion of the elastic element in the corresponding subsystem.

2 Subsystems composition

The model implementing the X–T coupling type was already detailed and its results already examined in a previous paper [27]. Since then, the X–X coupling type was implemented without modifying the modeling choices previously made. This model will therefore be briefly reminded in the present section.

The vehicle–track–soil model is composed of 4 subdomains spread into 2 subsystems. Since the recoupling is performed at the ballast level using applied-force co-simulation techniques, both subsystems are defined as follows:

- The *upper* (or vehicle) subsystem contains the vehicle, rail and sleepers' subdomains. Implicitly, this means that the coupling elements in-between (the wheel/rail contact and the railpads) are also included. The complete modeling of this subsystem is performed in two-dimensions due to the symmetry of the system. This two-dimensional modeling of the vehicle limits the system since the results obtained will be valid for straight motion only. In order to simulate the effect of lateral displacement of the vehicle or curved motion, a three-dimensional modeling would be required. All equations representing the vehicle behavior, given in Eqs. (1a), (1b), (1c), are implemented in an in-house multibody dedicated software called EasyDyn [29, 30].
- The *lower* (or soil) subsystem contains the soil. The modeling of this subsystem is performed in three-dimensions. The third dimension becomes mandatory for vibration assessment along the direction perpendicular to the track. The soil, whose general form of equations is given in Eq. (2), is modeled and solved in Abaqus [31], a commercial finite element analysis software.

The upper subsystem is illustrated in Fig. 2. It can be noticed that the track is divided into three sections whose central one is coupled with the lower subsystem. The sections located at both extremities are used to perform a static equilibrium of the vehicle and its

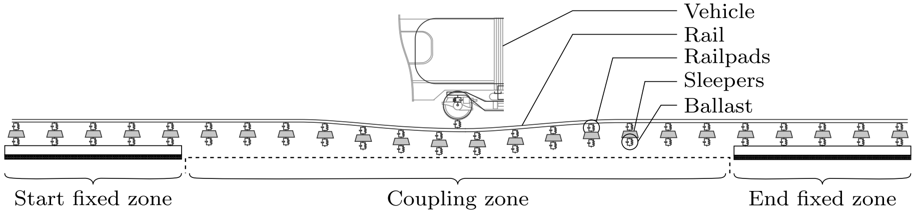

Fig. 2 Representation of the vehicle (upper) subsystem included in EasyDyn for a split at the ballast level. The dashed (– – –) line represents the separation between EasyDyn and Abaqus. The start and end regions are completely included in EasyDyn

track while considering that the soil is not directly affected by the vehicle and track weights. For the sake of clarity, the proportions between the lengths of the three zones were not kept for Fig. 2. In the actual modeling, the start and end zones are approximately 8 times smaller than the coupling that contains 81 sleepers spaced by 0.6 meters. The useful length is therefore around 48 meters. Compared to usual bogie sizes and considering that only one axle is used for the vehicle modeling, the coupling zone size remains reasonable for ground-borne vibration assessment [32].

The motion of the vehicle is described using the minimal coordinates' approach through homogeneous transformation matrices. The equations of motion of the vehicle subdomain are then automatically derived by a symbolic tool and written in C++ in such a way that it can be time-integrated with EasyDyn. In this paper, however, the vehicle is a single axle with its two wheels whose motion is allowed in the vertical direction only. The vehicle is genuinely simplified to focus on the effect of co-simulation techniques applied to railway dynamics problems including a more comprehensive modeling of the soil. Furthermore, the equations of motion of the vehicle can be written in a generic form expressed in Eq. (1a) where $\overrightarrow{\mathbf{q}}_v$, $\overrightarrow{\dot{\mathbf{q}}}_v$, and $\overrightarrow{\ddot{\mathbf{q}}}_v$ represent the vehicle configuration parameters and their first and second time derivatives, respectively. This notation will be kept in the following lines. The matrix $\mathbf{M}_v(\overrightarrow{\mathbf{q}}_v)$ contains the mass and inertial terms. The vector $\overrightarrow{\mathbf{h}}_v$ represents the Coriolis, gyroscopic, and centrifugal contributions, while $\overrightarrow{\mathbf{g}}_v$ contains the applied forces. It can be seen that this specific term is a function of $f_{r/v}$, which is a scalar containing the reaction of the rail on the vehicle. This reaction force comes from the wheel/rail contact that is defined using the nonlinear Hertz contact theory [33].

The rail is entirely composed of Euler–Bernoulli beam elements connected by nodes whose motion is described by two degrees of freedom: one for the vertical motion of each node and one for the rotation of each node about the horizontal axis perpendicular to the rail. All rail degrees of freedom are concatenated in the vector $\overrightarrow{\mathbf{q}}_r$. The Euler–Bernoulli beam theory provides the local stiffness and mass matrices of each element located between two nodes. By assembling these local matrices, the global stiffness $\mathbf{K}_{r,\text{glob}}$ and mass $\mathbf{M}_{r,\text{glob}}$ matrices are recovered. The equations of motion of the rail subdomain are expressed in Eq. (1b). Besides the weight of the rail nodes, denoted by $\overrightarrow{\mathbf{g}}_r$, the vector of reaction force of the sleepers $\overrightarrow{\mathbf{f}}_{s/r}$ and the action force of the vehicle $\overrightarrow{\mathbf{f}}_{v/r}$ are taken into account in the rail equation set. The vector of reaction force of the sleepers $\overrightarrow{\mathbf{f}}_{s/r}$ is computed considering that the railpads are elastic and damped elements that link one sleeper with one specific rail node as depicted in Fig. 2, or further in the paper in Figs. 4 and 5. The railpads are supposed to have a linear behavior described by k_p stiffness and d_c damping coefficients. The action force of the vehicle $\overrightarrow{\mathbf{f}}_{v/r}$, derived from the scalar $f_{r/v}$ evoked in the vehicle subdomain

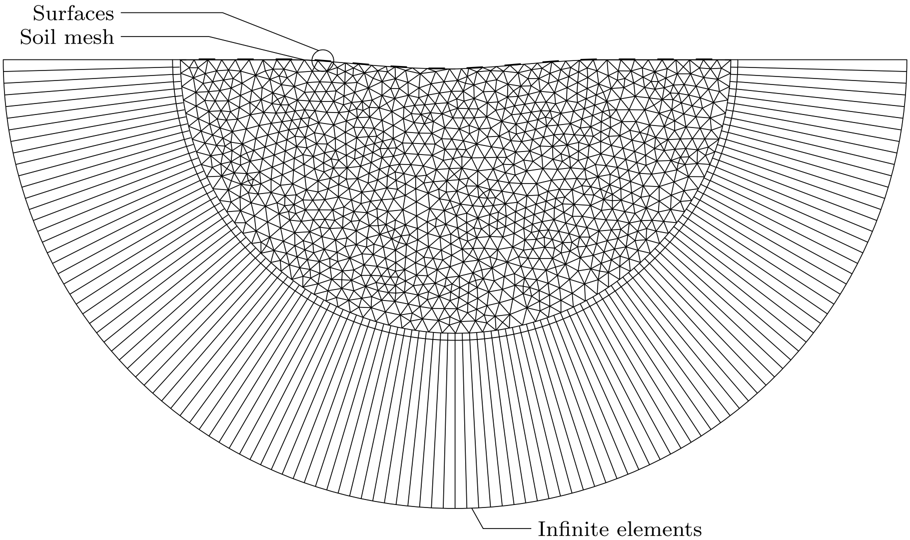

Fig. 3 Representation of the soil (lower) subsystem included in ABAQUS for a split at the ballast level

composition, is sprayed on the rail nodes using shape functions as described by Nielsen et al. [34].

Among other things, the stability of the rails and their parallelism are insured, in this model, by concrete sleepers. Due to their limited motion, each sleeper is here modeled by lumped masses whose motion is entirely represented by a vertical degree of freedom. Therefore, with m_s being the mass of a sleeper, the set of equations of motion of all the sleepers is summarized in Eq. (1c). Their weight $\vec{\mathbf{g}}_s$ is also taken into account. As it was considered in the rail subdomain equations set, the action of the rail exerted through the railpads is represented by the term $\vec{\mathbf{f}}_{r/s}$:

$$\mathbf{M}_v(\vec{\mathbf{q}}_v)\ddot{\vec{\mathbf{q}}}_v + \vec{\mathbf{h}}_v(\vec{\mathbf{q}}_v, \dot{\vec{\mathbf{q}}}_v) - \vec{\mathbf{g}}_v(\vec{\mathbf{q}}_v, \dot{\vec{\mathbf{q}}}_v, t, f_{r/v}) = 0, \tag{1a}$$

$$\mathbf{M}_{r,\text{glob}}\ddot{\vec{\mathbf{q}}}_r + \mathbf{K}_{r,\text{glob}}\vec{\mathbf{q}}_r - \vec{\mathbf{f}}_{v/r} - \vec{\mathbf{f}}_{s/r} - \vec{\mathbf{g}}_r = 0, \tag{1b}$$

$$m_s\ddot{\vec{\mathbf{q}}}_s - \vec{\mathbf{f}}_{r/s} - \vec{\mathbf{f}}_{g/s}\left(\vec{\mathbf{u}}_{\text{ED}}\right) - \vec{\mathbf{g}}_s = 0. \tag{1c}$$

The term $\vec{\mathbf{f}}_{g/s}\left(\vec{\mathbf{u}}_{\text{ED}}\right)$, given in the set of equations providing the sleepers motion, represents the force developed by the ground surface on the sleepers through the ballast. As in the case of the railpads, the ballast is, in this model, considered as a set of independent, elastic, and damped elements acting on each sleeper. This can be seen in Fig. 2. Again, the behavior of the ballast elements is linearly defined by stiffness and damping coefficients denoted k_b and d_b, respectively. In the upper subsystem, the forces exerted through the ballast directly depend on the dynamics of the lower subsystem. Hence, these forces are functions of the coupling variables. Their nature (kinematic or force quantities) being not clearly defined for now, these coupling variables are defined as EASYDYN inputs $\vec{\mathbf{u}}_{\text{ED}}$.

Unlike the vehicle subsystem, the soil subsystem is, on the one hand, modeled and solved in a finite element analysis software and, on the other hand, it is modeled in three dimensions since its intrinsic purpose is ground-borne vibration assessment. As depicted in Fig. 3, the soil is divided in two different parts, namely the soil mesh and an envelope of infinite elements. The soil is supposed to be homogeneous and its characteristics are completely defined by Young's modulus E, Poisson's coefficient ν, density ρ, and viscous damping coefficient β. This soil construction, detailed in [7], is performed to model the infinity of the soil as well as to avoid undesirable wave reflection at the boundary between the soil mesh and its envelope. Figure 3 also shows that rigid surfaces are created at the ground surface. The motion of these rigid surfaces is then reduced to the motion of their center point to facilitate the coupling with the sleepers contained in the upper subsystem. The residual form of the equations of motion representing the soil motion can be symbolized by Eq. (2) where the vector $\vec{\mathbf{q}}_{g,\mathrm{tot}}$ represents the whole set of degrees of freedom of the soil. This vector necessarily includes the specific degrees of freedom describing the motion of the ground surfaces, denoted by $\vec{\mathbf{q}}_g^{\,c}$ in the rest of the paper,

$$\vec{\mathbf{r}}_g\left(\ddot{\vec{\mathbf{q}}}_{g,\mathrm{tot}}, \dot{\vec{\mathbf{q}}}_{g,\mathrm{tot}}, \vec{\mathbf{q}}_{g,\mathrm{tot}}, \vec{\mathbf{f}}_{s/g}\left(\vec{\mathbf{u}}_{\mathrm{Ab}}\right)\right) = 0. \tag{2}$$

The coupling between both subsystems is represented by the action force of the sleepers on the rigid surfaces through the ballast. In Eq. (2), this contribution is symbolized by the vector $\vec{\mathbf{f}}_{s/g}(\vec{\mathbf{u}}_{\mathrm{Ab}})$. As in the sleepers equation set, these forces are functions of the ABAQUS inputs $\vec{\mathbf{u}}_{\mathrm{Ab}}$.

The definition of the forces exerted through the ballast $\vec{\mathbf{f}}_{g/s}(\vec{\mathbf{u}}_{\mathrm{ED}})$ and $\vec{\mathbf{f}}_{s/g}(\vec{\mathbf{u}}_{\mathrm{Ab}})$ is given in the following section.

3 Subsystems interaction

Regarding the co-simulation schemes, both Jacobi (parallel) and Gauß–Seidel (sequential) approaches are implemented between EASYDYN and ABAQUS. In order to emphasize the effect of co-simulation on the results, a noniterative zeroth-order hold (ZOH) [35] method is kept. While, in the parallel approach, both subsystems are time-integrated simultaneously, it is not the case in the sequential approach. Moreover, the co-simulation master being implemented within the upper subsystem, the choice was made to time-integrate the upper subsystem before the lower subsystem.

The principal aim of this paper is to investigate the effect of the co-simulation type which defines the nature of the coupling variables exchanged between the subsystems at each macrotimestep. As it was already described in [27], using applied-force co-simulation techniques in the vehicle–track–soil model leads to two different options (theoretically described by Busch [11]) for the nature of the coupling variables:

– A *displacement/force* (X–T) coupling: in this case, the upper subsystem receives a kinematic quantity (X) from the lower subsystem. The coupling element is hence explicitly defined in the upper subsystem. The lower subsystem, however, receives the force (T) exerted through the coupling element computed in the upper subsystem.
– A *displacement/displacement* (X–X) coupling: in this case, both the upper and lower subsystems receive a kinematic quantity (X) from the other one. The coupling element is hence defined in both subsystems.

Practically, in the vehicle–track–soil model implemented with the X–T type, the vehicle subsystem receives, for sleeper i, the displacement $q^c_{g,i}$ and velocity $\dot{q}^c_{g,i}$ of the rigid surface i created at the ground surface, using the motion of its center point. The force $f^c_{s,i/g,i}$ developed by the ballast element i, which links center point i with its corresponding sleeper

Fig. 4 Focus on coupling element i of the X–T coupling type used in the vehicle–track–soil modeling with a split at the ballast level. Figure from [27]

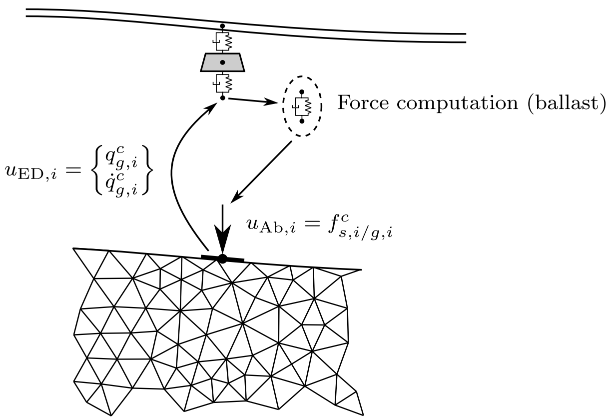

i, is computed such that it can be shared with the soil subsystem. This force applied by the sleeper on the soil is transformed into a pressure to be applied on the specific soil rigid surface. An illustration of this methodology is presented in Fig. 4.

In the X–T case, the inputs of the vehicle subsystem also called EasyDyn inputs $\vec{\mathbf{u}}_{\mathrm{ED}}$ are given in Eq. (3a). These inputs correspond to the vectors of displacements $\vec{\mathbf{q}}^{\,c}_{g}$ and velocities $\dot{\vec{\mathbf{q}}}^{\,c}_{g}$ of the rigid surfaces created on the soil. The inputs of the soil, also called Abaqus inputs $\vec{\mathbf{u}}_{\mathrm{Ab}}$, given in Eq. (3b), are the forces $\vec{\mathbf{f}}^{\,c}_{s/g}$ applied by the sleepers through the ballast on the soil in the coupling region:

$$\vec{\mathbf{u}}_{\mathrm{ED}} = \begin{bmatrix} \vec{\mathbf{q}}^{\,c}_{g} \\ \dot{\vec{\mathbf{q}}}^{\,c}_{g} \end{bmatrix}, \tag{3a}$$

$$\vec{\mathbf{u}}_{\mathrm{Ab}} = \vec{\mathbf{f}}^{\,c}_{s/g}. \tag{3b}$$

The computation of the forces $\vec{\mathbf{f}}_{g/s}$ developed by the ballast is detailed in Eq. (4) for the upper subsystem. It can be seen that it is split into three different regions: the start, coupling, and end regions denoted by s, c, and e, respectively. As depicted in Fig. 2, the soil in the start and end regions is supposed to be perfectly rigid in such a way that the displacements and velocities are null:

$$\vec{\mathbf{f}}_{g/s} = \begin{Bmatrix} \vec{\mathbf{f}}^{\,s}_{g/s} \\ \vec{\mathbf{f}}^{\,c}_{g/s} \\ \vec{\mathbf{f}}^{\,e}_{g/s} \end{Bmatrix} = -k_b \left(\vec{\mathbf{q}}_{s} - \begin{Bmatrix} 0 \\ \vec{\mathbf{q}}^{\,c}_{g} \\ 0 \end{Bmatrix} \right) - d_b \left(\dot{\vec{\mathbf{q}}}_{s} - \begin{Bmatrix} 0 \\ \dot{\vec{\mathbf{q}}}^{\,c}_{g} \\ 0 \end{Bmatrix} \right). \tag{4}$$

In the vehicle–track–soil model implemented with the X–X type, the vehicle subsystem still receives, for sleeper i, the displacement $q^c_{g,i}$ and velocity $\dot{q}^c_{g,i}$ of the rigid surface i. The soil subsystem, however, receives the displacement $q^c_{s,i}$ and velocity $\dot{q}^c_{s,i}$ of the corresponding sleeper i. In this case, the ballast is explicitly implemented in both subsystems in such a way that the developed force is computed independently in both subsystems. This violates the action–reaction principle, but this violation decreases with the macrotimestep reduction. Figure 5 shows a representation of the X–X methodology.

In the X–X type of co-simulation, the inputs of the upper subsystem $\vec{\mathbf{u}}_{\mathrm{ED}}$, summarized in Eq. (5a), are still the displacements $\vec{\mathbf{q}}^{\,c}_{g}$ and velocities $\dot{\vec{\mathbf{q}}}^{\,c}_{g}$ of the ground surfaces in

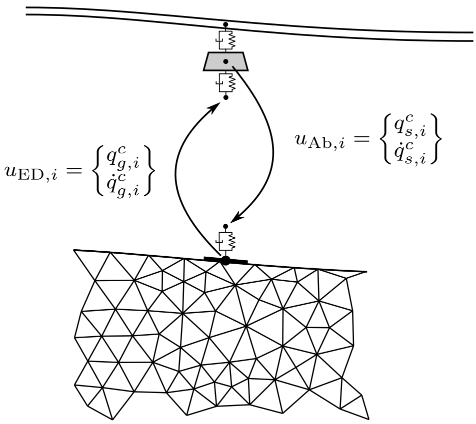

Fig. 5 Focus on coupling element i of the X–X coupling type used in the vehicle–track–soil modeling with a split at the ballast level

the coupling region. The inputs of the lower subsystem $\vec{\mathbf{u}}_{\mathrm{Ab}}$, given in Eq. (5b), are the displacements $\vec{\mathbf{q}}^{\,c}_{s}$ and velocities $\dot{\vec{\mathbf{q}}}^{\,c}_{s}$ of the sleepers in the coupling region:

$$\vec{\mathbf{u}}_{\mathrm{ED}} = \begin{bmatrix} \vec{\mathbf{q}}^{\,c}_{g} \\ \dot{\vec{\mathbf{q}}}^{\,c}_{g} \end{bmatrix}, \tag{5a}$$

$$\vec{\mathbf{u}}_{\mathrm{Ab}} = \begin{bmatrix} \vec{\mathbf{q}}^{\,c}_{s} \\ \dot{\vec{\mathbf{q}}}^{\,c}_{s} \end{bmatrix}. \tag{5b}$$

4 Implemented co-simulation strategy

Even though the co-simulation strategy was largely developed in [27], a major improvement is presented in this paper, namely an implementation of the X–X co-simulation type between EASYDYN and ABAQUS. The main aim of this paper is then to present and study the application of both X–T and X–X types to a co-simulated vehicle/track/soil modeling dedicated to ground-borne vibration assessment. Figure 6 illustrates the co-simulation strategy implemented to allow Jacobi and Gauß–Seidel schemes with X–T and X–X types between EASYDYN and ABAQUS. This remains a single-rate co-simulation method with a common macrotimestep, each subsystem having its own adaptive microtimestep.

Regarding the actual communication between both software packages, no specific FMI protocol [36] is used. Instead, an in-house TCP/IP based methodology is preferred for the sake of simplicity in the implementation. The details of the different steps presented in Fig. 6, given in [27], are briefly summarized below:

– *Step 0* (executed once). The model is loaded in ABAQUS and the user-defined subroutines are linked. Meanwhile, the model is loaded in EASYDYN and the static equilibrium of the vehicle subsystem is performed while considering that the soil is fixed in the coupling region as well.
– *Step 1* (repeated). Both subsystems exchange their data also called coupling variables above. The TCP/IP communication is highlighted and both Jacobi $\vec{\mathbf{u}}^{\,\mathrm{J}}_{\mathrm{Ab}}$ and Gauß–Seidel $\vec{\mathbf{u}}^{\,\mathrm{GS}}_{\mathrm{Ab}}$ inputs are distinguished.

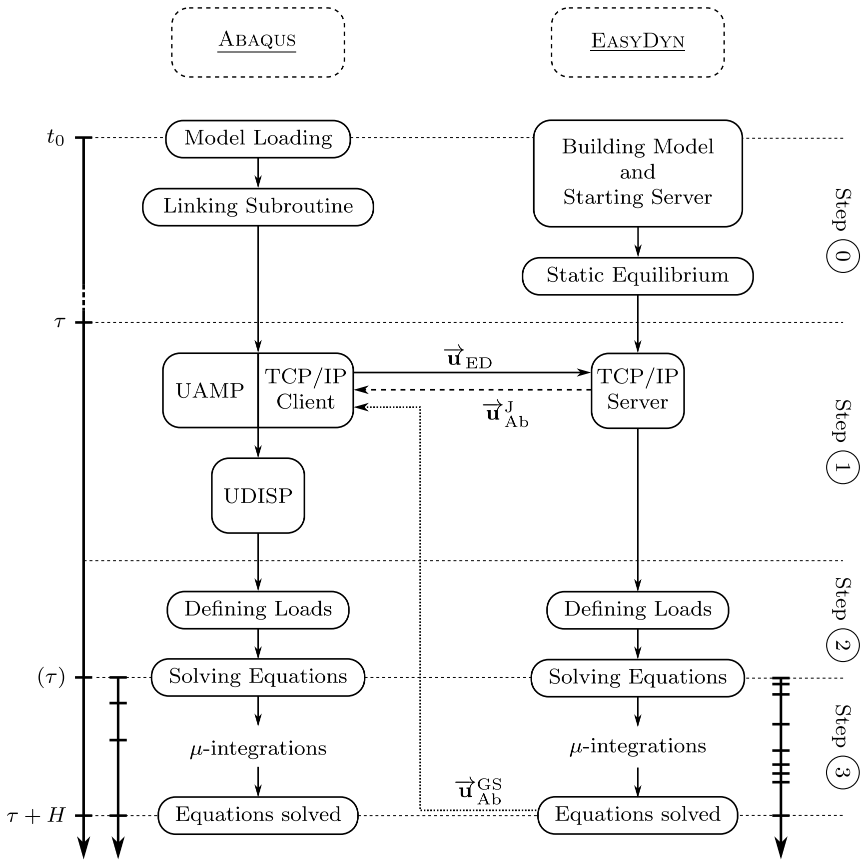

Fig. 6 Workflow steps for ABAQUS (Ab) and EASYDYN (ED) interaction during co-simulation for both X–T and X–X coupling type. Plain (——), dashed (- - -), and dotted (······) arrows depict common, Jacobi (J), and Gauß–Seidel (GS) workflows, respectively. Figure adapted from [27]

- *Step 2* (repeated). The loads are defined by taking into account the coupling variables previously exchanged.
- *Step 3* (repeated). Both subsystems are time-integrated using their respective solvers.

The actual contribution of the model presented in this paper relies in Step 1 of the co-simulation workflow depicted in Fig. 6. To be more specific, the call of the `UDISP` user-subroutine [37] provides a way to impose the displacements and velocities of the "unconnected" nodes of the ballast elements modeled in the soil subsystem. In this case, these "unconnected" nodes represents the sleepers motion in the soil subsystem. The call of the `UAMP` user-subroutine is, however, mandatory since:

- it contains the TCP/IP client that communicates with the server started by the co-simulation master implemented in EASYDYN and
- it defines ABAQUS "Amplitudes".

These "Amplitudes" are stored in a memory shared by the whole ABAQUS program. This way, these amplitudes can be linked to the definition of the forces applied on the rigid sur-

Table 1 Parameters defining the upper subsystem

Component	Parameter	Symbol	Value	Unit
Wheelset	Mass	m_v	10	T
	Speed	v_0	300	km/h
Contact	Hertz contact stiffness	k_{Hz}	92.86	GN/m
Rail	Section	A_r	63.8	cm^2
	Geometrical moment of inertia	I_r	1987.8	cm^4
	Young's modulus	E_r	210	GPa
	Density	ρ_r	7800	$\mathrm{kg/m}^3$
	Number of rail elements per sleeper	$n_{r/s}$	2	–
Railpads	Stiffness	k_p	180	MN/m
	Damping	d_p	28	kNs/m
Sleeper	Number of sleepers in start zone	$n_{s,start}$	10	–
	Number of sleepers in coupling zone	$n_{s,CS}$	81	–
	Number of sleepers in end zone	$n_{s,end}$	10	–
	Mass	m_s	90.84	kg
	Spacing	L_s	0.6	m

Table 2 Parameters defining the coupling element

Component	Parameter	Symbol	Value	Unit
Ballast	Stiffness	k_p	25.5	MN/m
	Damping	d_p	40	kNs/m

faces created on the ground in the X–T case. In the X–X case, the `UDISP` subroutine is called after the `UAMP` in such a way that the kinematic quantities, stored in the amplitudes shared memory, can be used to impose the motion of the ballast "unconnected" nodes.

5 Ballast forces and soil motion

The model and its improvement being defined, it is now relevant to show and analyze the results obtained. Since the final aim of the model is to assess ground-borne vibrations, a specific attention is paid to the soil motion. First, an investigation of the motion of the soil at the level of the track, and so at the level of the coupling, is proposed. The motion of the soil observed along a direction perpendicular to the track will be treated further in this paper. For the sake of comparison, the parameters defining the model remain identical to the previously published X–T model [27]. These parameters, originally coming from Kouroussis et al. [38], are reminded in Tables 1, 2, and 3.

Further in the paper, a velocity-based indicator called the Peak Particle Velocity is used to quantify the ground-borne vibrations. Therefore, Fig. 7 depicts the time history of the velocities $\dot{q}_{g,\mathrm{mid}}$ of the soil surface (center point) under the mid-track sleeper for both X–T and X–X co-simulation types (columns) and for the three soil flexibilities (rows) specified in Table 3. Since it was already observed that decreasing the macrotimestep leads to a convergence of the results [27], the reference to compare the results with is the Gauß–Seidel

Table 3 Parameters defining the lower subsystem

Component	Parameter	Symbol	Value	Unit
Soil	Young's modulus (soft soil)	E	10	MPa
	Young's modulus (medium soil)	E	155	MPa
	Young's modulus (hard soil)	E	750	MPa
	Poisson's coefficient	ν	0.25	–
	Viscous damping	β	0.0004	s
	Density	ρ	1540	kg/m^3

scheme with an X–T type and a macrotimestep of 10^{-4} s. The compared results are, however, obtained using a macrotimestep of 10^{-3} s, each subsystem having its own adaptive microtimestep. This macrotimestep was specifically chosen because it is the largest admissible to accurately model the considered frequency range. The macrotimestep is therefore manually adaptable while the microtimesteps of each subsystem are not directly controllable since they are tuned by specific adaptive numerical methods. Briefly, EasyDyn uses a Newmark-$\frac{1}{4}$ implicit numerical scheme (trapezoidal rule) that does not introduce any damping in the results. In this case, the microtimestep is automatically adapted to reach a convergence of the results. In Abaqus, the Hilber–Hugues–Taylor (HHT-α) method is used with the standard parameters of the program. Moreover, the microtimestep is in this case set by the internal timestep manager of Abaqus.

Generally speaking, the difference between the results, and hence the effect of co-simulation, decreases with an increase of the Young's modulus of the soil. The stiffer the soil, the closer the results. A major difference can be spotted in Figs. 7a and 7b between X–T and X–X types. Indeed, for softer soils, where co-simulation effects significantly appear, it is observed that the results obtained using an X–X type with the Jacobi scheme are stable while they are not with an X–T type. It also appears that the X–X type provides more damped results than the X–T one. This overdamping phenomenon seems also amplified by the Jacobi scheme and might be due to the presence of the damping element in both subsystems.

Figure 8 shows the time history of the force applied $f_{s/g,\mathrm{mid}}$ by the mid-track sleeper on the soil. To obtain these results, a Gauß–Seidel co-simulation scheme is chosen with a macrotimestep of 10^{-3} s, mainly for its stability. In the X–T type, there is only one force represented in the graphs since it is the exchange variable that is used as input for the lower subsystem. In the X–X type, two values of the forces exerted through the ballast are computed due to the explicit definition of the coupling element in both subsystems. The difference between both computation of the forces is easily spotted in Figs. 8a and 8b for soft soil cases as well. As for sleeper velocities, this difference decreases with an increase of the soil rigidity. The stiffer the soil, the closer the forces.

6 Vehicle motion

Regarding the vehicle motion, the time history of the vertical displacement q_v of the vehicle is presented in Fig. 9. Both X–T (left) and X–X (right) co-simulation types are shown with both Jacobi and Gauß–Seidel schemes. Two different macrotimesteps are used, namely 1.10^{-4} and 1.10^{-3} s. Since the soft soil case appeared to be the most perturbed by co-simulation techniques, the medium and hard soil cases are avoided for the sake of clarity.

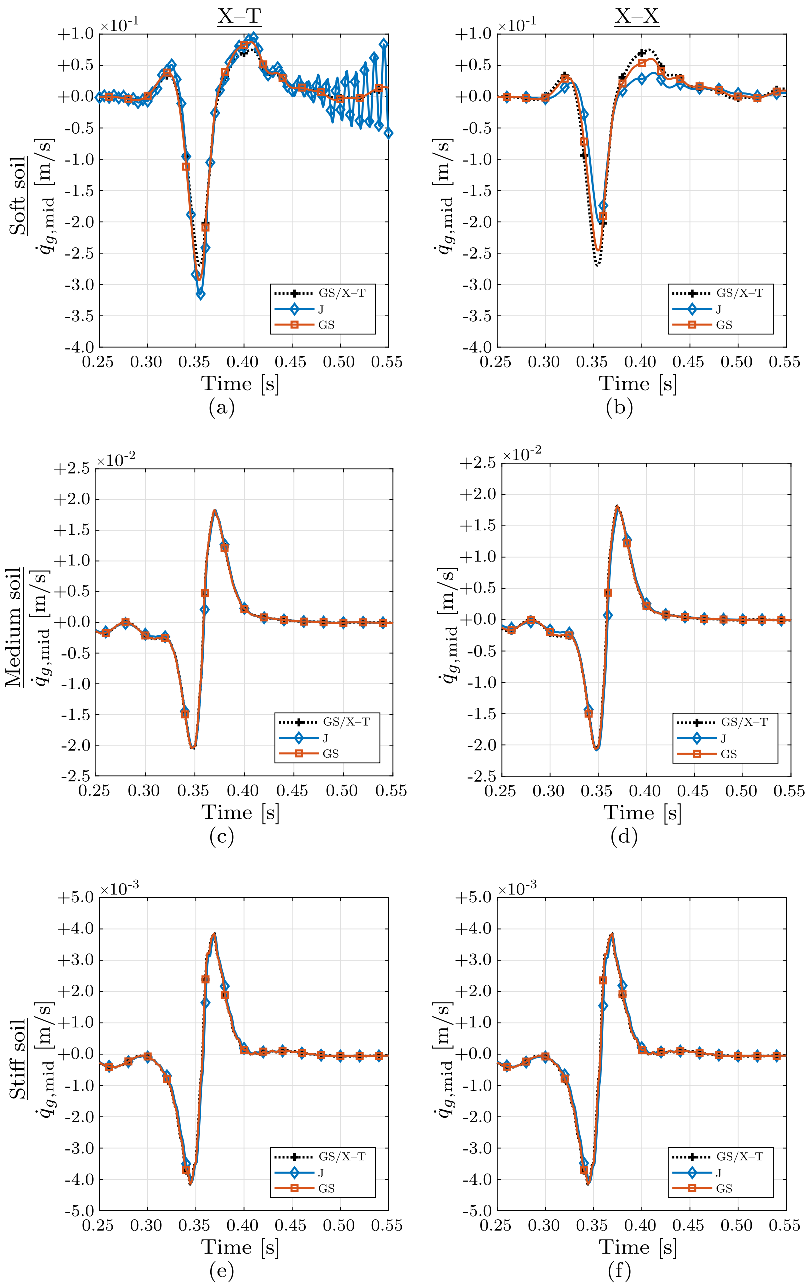

Fig. 7 Time history of the velocities $\dot{q}_{g,\mathrm{mid}}$ of the soil surface (center point) under the mid-track sleeper. Results for both X–T and X–X coupling types and both Jacobi (J) and Gauß–Seidel (GS) approaches. The dotted (- ·+- ·) curves are the GS-1.10^{-4} X–T reference.

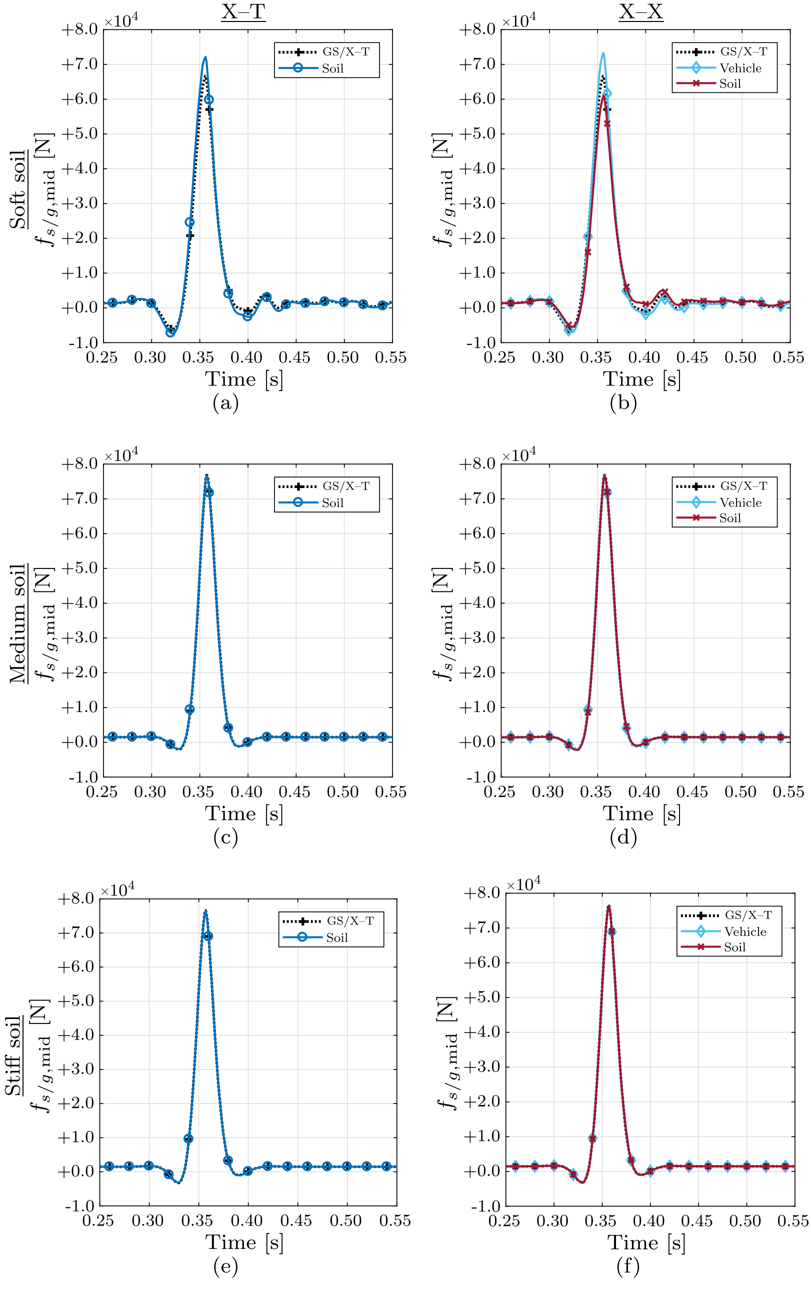

Fig. 8 Time history of the force applied $f_{s/g,\mathrm{mid}}$ by the mid-track sleeper on the soil. Results for both X–T and X–X coupling types with Gauß–Seidel (GS) approaches. The dotted (- -+- -) curves are the GS-1.10^{-4} X–T reference.

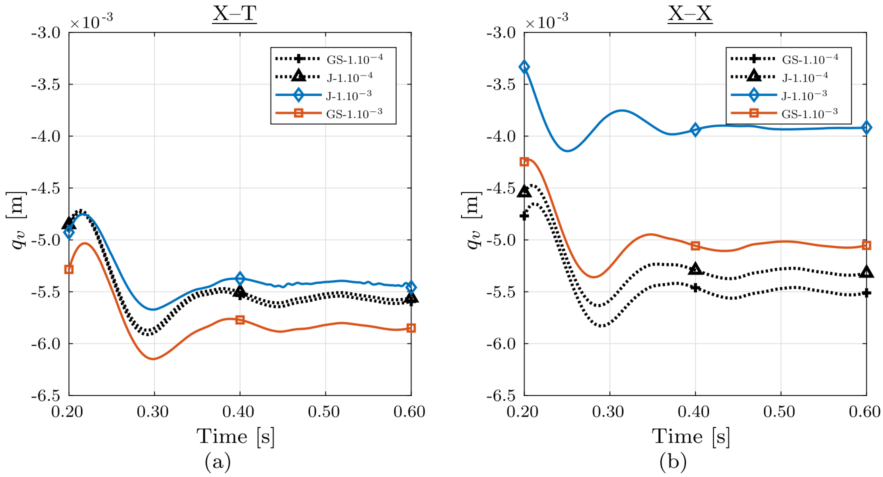

Fig. 9 Time history of the vehicle vertical displacement q_v for both X–T and X–X types. For the soft soil case only, Gauß–Seidel (GS) and Jacobi (J) schemes are represented with macrotimesteps of 10^{-4} and 1.10^{-3} s

Jacobi, used with a macrotimestep of 1.10^{-3} s and an X–T type, exhibited an unstable behavior at the level of the soil in Fig. 7a. In Fig. 9a, it can be pointed out that this unstable behavior does not appear as clearly from the point of view of the vehicle subsystem. This simulation remains, however, unstable.

The results obtained using a macrotimestep of 1.10^{-4} s appear to converge to a unique solution. This convergence turns out to be faster in the X–T case. This might be justified by the lack of accuracy created by the repetition of the coupling element in the X–X case, which leads to a violation of the action–reaction principle. Therefore, the GS/X–T-1.10^{-4} case is usually kept as a reference to compare with the other results.

Moreover, while comparing for both X–T and X–X types the results obtained with 1.10^{-4} and 1.10^{-3} s macrotimesteps, it appears that the X–T case is more accurate while the X–X case provides more stability.

7 Ground-borne vibration assessment

The principal aim of this model being to assess ground-borne vibrations, it is interesting to examine the Peak Particle Velocity [39] abbreviated by PPV. This indicator consists of the peak instantaneous velocity of the signal as given in Eq. (6a) where v_i denotes the projection of the velocity on direction i. In the case of the present model, the vertical velocity v_z remains predominant and the PPV can be computed as in Eq. (6b):

$$\mathrm{PPV_{tot}} = \max\left(\sqrt{v_x^2 + v_y^2 + v_z^2}\right), \tag{6a}$$

$$\mathrm{PPV_{tot}} = \max\left(\|v_z\|\right). \tag{6b}$$

Figure 10 provides the PPV with respect to the distance from track for the soft soil case with an X–T type. Gauß–Seidel and Jacobi approaches are represented with 1.10^{-4} and 1.10^{-3} s macrotimesteps. By plotting the PPV, the instability of Jacobi, X–T with a 1.10^{-3} s

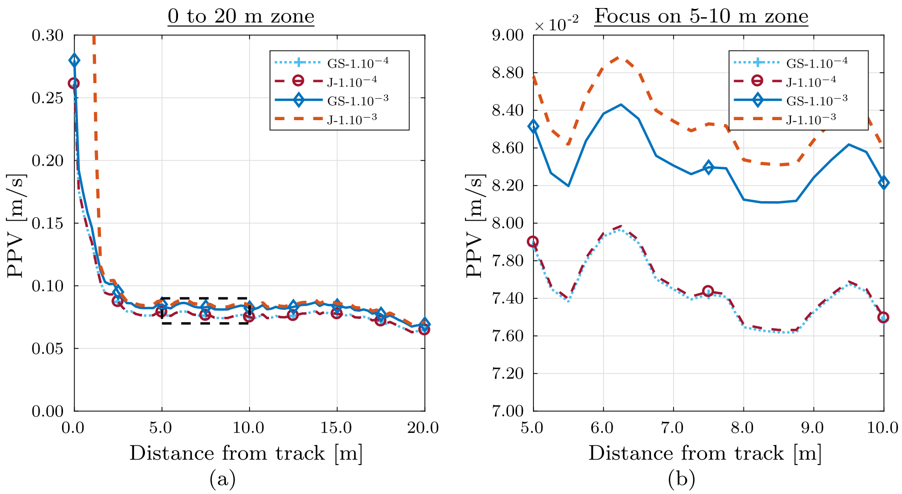

Fig. 10 Peak Particle Velocity with respect to the distance from track for soft soil case with an X–T type. Gauß–Seidel (GS) and Jacobi (J) schemes are represented with macrotimesteps of 10^{-4} and 1.10^{-3} s

macrotimestep, is immediately spotted. Except for this Fig. 10, the results are not explicitly represented in the rest of the paper for the sake of clarity. It can be seen that unrealistic values are obtained near the track but more realistic values are still obtained further for Jacobi, X–T with a 1.10^{-3} s macrotimestep. This is due to the fact that the total simulation time is not large enough, in this case, to let the instability propagate through the soil surface.

Figure 10b exhibits the proximity of the results obtained using both Jacobi and Gauß–Seidel approaches with a macrotimestep of 1.10^{-4} s. Once again, it is shown that decreasing the macrotimestep leads to a convergence in the solutions. Moreover, it appears that, while Gauß–Seidel with a macrotimestep of 1.10^{-3} s provides comparable (slightly overestimated) results but for a computational burden reduced by a factor of approximately 10.

The comparison of the PPV obtained for X–T and X–X cases is provided in Fig. 11. Both Gauß–Seidel and Jacobi are used with a macrotimestep of 1.10^{-3} s and the results are compared with the Gauß–Seidel approach with an X–T type and a macrotimestep of 1.10^{-4} s.

It is immediately noticed that, while Jacobi is unstable in the X–T case, it is stable in the X–X one. The results obtained using the X–X type are, however, significantly underestimated by the Jacobi approach. Moreover, looking at the Gauß–Seidel results, the difference between the X–X type and the reference is slightly larger than the difference between the X–T type and the reference. The tendency observed for the ballast forces and soil motion in Sect. 5 remains appropriate: if the X–X type stabilize the simulation, the results obtained exhibits a more damped behavior.

8 Conclusions

A specific attention must be paid on the choice of the coupling type when building a co-simulated vehicle–track–soil model. Indeed, both displacement/displacement (X–X) and displacement/force (X–T) coupling types have their specific effect on the results obtained.

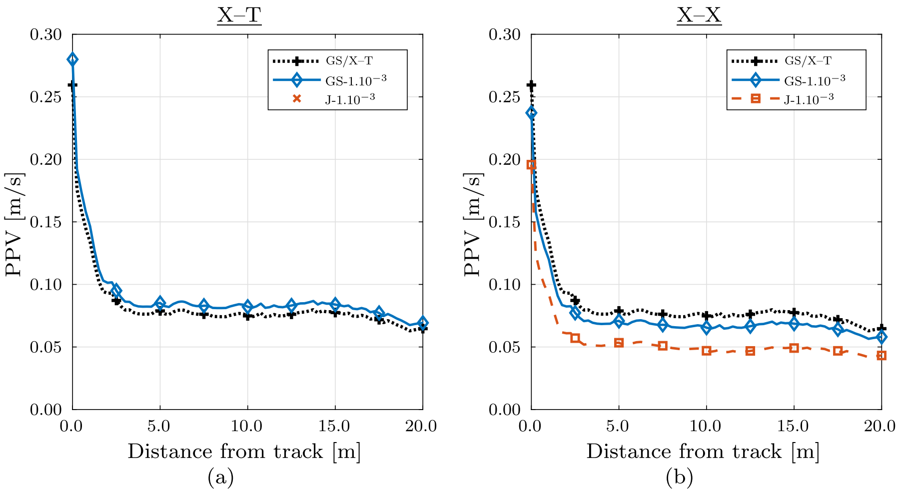

Fig. 11 Peak Particle Velocity with respect to the distance from track for soft soil case. Gauß–Seidel (GS) and Jacobi (J) schemes are represented with macrotimestep of 1.10^{-3} s. A cross ($\times$) in the legend depicts unstable results

After describing the general construction of the model, this paper presented a possible way to implement co-simulation between an in-house multibody dedicated software and a commercial finite element analysis software using either X–T or X–X type. This co-simulation, being noniterative and zeroth-order hold, included the management of Jacobi and Gauß–Seidel approaches.

The velocity of the soil point located below the mid-track sleeper was observed, as well as the force exerted on this specific point through the ballast element. It appeared that using a displacement/displacement type provides a stabilizing effect since Jacobi was stable in this case but not in the displacement/force type while keeping the same macrotimestep. This instability of the Jacobi approach also appeared to be still present but less significant in the displacement of the vehicle. However, computing the PPV gave an undeniable indicator of instability. Besides, the displacement/displacement type of coupling exhibited a certain lack of accuracy, especially in the time history of the vehicle displacement and in the PPV. In any case, reducing the macrotimestep leads to a convergence of the results but at the price of a larger computational burden. This computational burden was not explicitly described in the paper since it does not differ from the simulation times obtained for the X–T type [27]. This is mainly due to the large asymmetry in terms of degrees of freedom between the upper and the lower subsystem (approximately a ratio of 1000 in-between). Indeed, the time integration of the soil subsystem remains predominant in the total simulation time.

Regarding ground-borne vibration assessment, the Gauß–Seidel approach used with the displacement/force type provided results considerably close to the same simulation executed with a macrotimestep 10 times smaller. For the vehicle–track–soil model, iterations over the macrotimesteps and extrapolation of the coupling variables remains solid perspectives to improve the accuracy of the results and the simulation stability for a larger macrotimestep. Moreover, several changes could be taken into account in order to improve the ability of the proposed model regarding vibration assessment. Mainly, a more comprehensive model of the vehicle including lateral motion or even curved trajectories would enrich the obtained results. This would, however, require to switch from a two- to a three-dimensional modeling of the vehicle subsystem with a more accurate description of the wheel/rail contact as well as a more accurate modeling of the rail, sleepers, railpads, and also ballast.

References

1. Thompson, D.J., Kouroussis, G., Ntotsios, E.: Modelling, simulation and evaluation of ground vibration caused by rail vehicles. Veh. Syst. Dyn. **57**(7), 936–983 (2019)
2. Stoura, C.D., Paraskevopoulos, E., Dimitrakopoulos, E.G., Natsiavas, S.: A dynamic partitioning method to solve the vehicle–bridge interaction problem. Comput. Struct. **251**, 106547 (2021)
3. Connolly, D., Giannopoulos, A., Forde, M.C.: Numerical modelling of ground borne vibrations from high speed rail lines on embankments. Soil Dyn. Earthq. Eng. **46**, 13–19 (2013)
4. Zhai, W., Sun, X.: A detailed model for investigating vertical interaction between railway vehicle and track. Veh. Syst. Dyn. **23**(sup1) (1994)
5. Zhai, W., He, Z., Song, X.: Prediction of high-speed train induced ground vibration based on train–track–ground system model. Earthq. Eng. Eng. Vib. **9**(4), 545–554 (2010)
6. Yang, J., Zhu, S., Zhai, W., Kouroussis, G., Wang, Y., Wang, K., Lan, K., Xu, F.: Prediction and mitigation of train-induced vibrations of large-scale building constructed on subway tunnel. Sci. Total Environ. **668**, 485–499 (2019)
7. Kouroussis, G., Van Parys, L., Conti, C., Verlinden, O.: Using three-dimensional finite element analysis in time domain to model railway-induced ground vibrations. Adv. Eng. Softw. **70**, 63–76 (2014)
8. Kouroussis, G., Connolly, D.P., Vogiatzis, K., Verlinden, O.: Modelling the environmental effects of railway vibrations from different types of rolling stock: a numerical study. Shock Vib. **2015**, 142807 (2015)
9. Kouroussis, G., Florentin, J., Verlinden, O.: Ground vibrations induced by InterCity/InterRegion trains: a numerical prediction based on the multibody/finite element modeling approach. J. Vib. Control **22**(20) (2016). https://doi.org/10.1177/1077546315573914
10. González, F., Naya, M.Á., Luaces, A., González, M.: On the effect of multirate co-simulation techniques in the efficiency and accuracy of multibody system dynamics. Multibody Syst. Dyn. **25**(4), 461–483 (2011)
11. Busch, M.: Zur effizienten Kopplung von Simulationsprogrammen. PhD thesis, Kassel University (2012)
12. Schweizer, B., Lu, D.: Semi-implicit co-simulation approach for solver coupling. Arch. Appl. Mech. **84**(12), 1739–1769 (2014)
13. Schweizer, B., Lu, D., Li, P.: Co-simulation method for solver coupling with algebraic constraints incorporating relaxation techniques. Multibody Syst. Dyn. **36**(1), 1–36 (2016)
14. Li, P.: On the numerical stability of co-simulation methods. PhD thesis, Darmstadt Technische Universität (2017)
15. Rahikainen, J., González, F., Naya, M.Á., Sopanen, J., Mikkola, A.: On the cosimulation of multibody systems and hydraulic dynamics. Multibody Syst. Dyn. **50**(2), 143–167 (2020)
16. Rahikainen, J., González, F., Naya, M.Á.: An automated methodology to select functional co-simulation configurations. Multibody Syst. Dyn. **48**(1) (2020). https://doi.org/10.1007/s11044-019-09696-y
17. Chen, W., Ran, S., Wu, C., Jacobson, B.: Explicit parallel co-simulation approach: analysis and improved coupling method based on H_∞ synthesis. Multibody Syst. Dyn. **52**, 255–279 (2021)
18. Dietz, S., Hippmann, G., Schupp, G.: Interaction of vehicles and flexible tracks by co-simulation of multibody vehicle systems and finite element track models. Veh. Syst. Dyn. **37**(sup1), 372–384 (2002)
19. Ambrósio, J., Pombo, J., Rauter, F., Pereira, M.: A memory based communication in the co-simulation of multibody and finite element codes for pantograph-catenary interaction simulation. In: Multibody Dynamics, pp. 231–252. Springer, Berlin (2009)
20. Massat, J.-P., Laurent, C., Bianchi, J.-P., Balmès, E.: Pantograph catenary dynamic optimisation based on advanced multibody and finite element co-simulation tools. Veh. Syst. Dyn. **52**(Suppl. 1), 338–354 (2014)
21. Antunes, P., Magalhães, H., Ambrósio, J., Pombo, J., Costa, J.: A co-simulation approach to the wheel–rail contact with flexible railway track. Multibody Syst. Dyn. **45**(2), 245–272 (2019)
22. Gomes, C., Thule, C., Broman, D., Larsen, P., Vangheluwe, H.: Co-simulation: State of the art (2017). arXiv:1702.00686
23. Gomes, C., Thule, C., Broman, D., Larsen, P., Vangheluwe, H.: Co-simulation: a survey. ACM Comput. Surv. **51**(3), 49 (2018)
24. Wu, Q., Sun, Y., Spiryagin, M., Cole, C.: Parallel co-simulation method for railway vehicle–track dynamics. J. Comput. Nonlinear Dyn. **13**(4), 041004 (2018)

25. Olivier, B., Verlinden, O., Kouroussis, G.: Effect of applied force cosimulation schemes on recoupled vehicle/track problems. Multibody Syst. Dyn. **50**(4), 337–353 (2020)
26. Costa, J.N., Antunes, P., Magalhães, H., Pombo, J., Ambrósio, J.: A finite element methodology to model flexible tracks with arbitrary geometry for railway dynamics applications. Comput. Struct. **254**, 106519 (2021)
27. Olivier, B., Verlinden, O., Kouroussis, G.: A vehicle/track/soil model using co-simulation between multibody dynamics and finite element analysis. Int. J. Rail Transp. **8**(2), 135–158 (2020)
28. Wang, J., Ma, Z.-D., Hulbert, G.M.: A gluing algorithm for distributed simulation of multibody systems. In: ASME 2003 International Design Engineering Technical Conferences and Computers and Information in Engineering Conference, pp. 89–104 (2003). American Society of Mechanical Engineers
29. Verlinden, O., Fékih, L.B., Kouroussis, G.: Symbolic generation of the kinematics of multibody systems in EasyDyn: from MuPAD to Xcas/Giac. Theor. Appl. Mech. Lett. **3**(1), 013012 (2013)
30. Olivier, B., Verlinden, O., Kouroussis, G.: A vehicle/track co-simulation model using EasyDyn. In: 7th International Conference on Computational Methods in Structural Dynamics and Earthquake Engineering, pp. 1–10. Hersonissos, Greece (2019)
31. Dassault Systèmes - Simulia. ABAQUS 6.13 Documentation, 2013
32. Kouroussis, G., Verlinden, O., Conti, C.: Free field vibrations caused by high-speed lines: measurement and time domain simulation. Soil Dyn. Earthq. Eng. **31**(4), 692–707 (2011)
33. Kouroussis, G., Verlinden, O., Conti, C.: On the interest of integrating vehicle dynamics for the ground propagation of vibrations: the case of urban railway traffic. Veh. Syst. Dyn. **48**(12), 1553–1571 (2010)
34. Nielsen, J.C.O., Abrahamsson, T.J.S.: Coupling of physical and modal components for analysis of moving non-linear dynamic systems on general beam structures. Int. J. Numer. Methods Eng. **33**(9), 1843–1859 (1992)
35. Peiret, A., González, F., Kövecses, J., Teichmann, M.: Multibody system dynamics interface modelling for stable multirate co-simulation of multiphysics systems. Mech. Mach. Theory **127**, 52–72 (2018)
36. Blockwitz, T., Otter, M., Akesson, J., Arnold, M., Clauss, C., Elmqvist, H., Friedrich, M., Junghanns, A., Mauss, J., Neumerkel, D., et al.: Functional mockup interface 2.0: the standard for tool independent exchange of simulation models. In: Proceedings of the 9th MODELICA Conference, Munich, Germany, pp. 173–184 (2012)
37. Dassault Systemes. Writing user subroutines with Abaqus
38. Kouroussis, G., Verlinden, O., Conti, C.: Influence of some vehicle and track parameters on the environmental vibrations induced by railway traffic. Veh. Syst. Dyn. **50**(4), 619–639 (2012)
39. Deutsches Institut für Normung. DIN 4150-3: Structural vibrations–Part 3: Effects of vibration on structures (1999)